


Ultrafast Exciton Dissociation Followed by Nongeminate Charge Recombination in PCDTBT:PCBM Photovoltaic Blends

Fabian Etzold,[†] Ian A. Howard,^{*,†} Ralf Mauer,[†] Michael Meister,[†] Tae-Dong Kim,[‡] Kwang-Sup Lee,^{*,‡} Nam Seob Baek,[§] and Frédéric Laquai^{*,†}

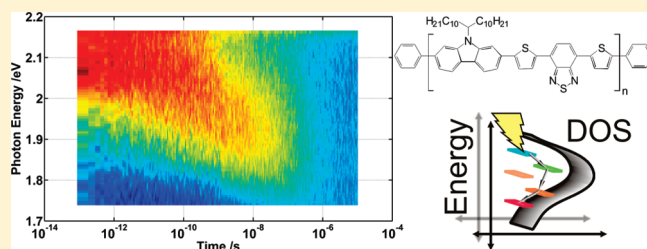
[†]Max Planck Research Group for Organic Optoelectronics, Max Planck Institute for Polymer Research, Ackermannweg 10, Mainz D-55128, Germany

[‡]Department of Advanced Materials, Hannam University, Daejeon 305-811, Republic of Korea

[§]IT Convergence Technology Research Laboratory, Electronics and Telecommunications Research Institute, Daejeon 305-700, Republic of Korea

 Supporting Information

ABSTRACT: The precise mechanism and dynamics of charge generation and recombination in bulk heterojunction polymer: fullerene blend films typically used in organic photovoltaic devices have been intensively studied by many research groups, but nonetheless remain debated. In particular the role of interfacial charge-transfer (CT) states in the generation of free charge carriers, an important step for the understanding of device function, is still under active discussion. In this article we present direct optical probes of the exciton dynamics in pristine films of a prototypic polycarbazole-based photovoltaic donor polymer, namely poly[*N*-11''-henicosanyl-2,7-carbazole-alt-5,5-(4',7'-di-2-thienyl-2',1',3'-benzothiadiazole)] (PCDTBT), as well as the charge generation and recombination dynamics in as-cast and annealed photovoltaic blend films using methanofullerene (PC₆₁BM) as electron acceptor. In contrast to earlier studies we use broadband (500–1100 nm) transient absorption spectroscopy including the previously unobserved but very important time range between 2 ns and 1 ms, which allows us not only to observe the entire charge carrier recombination dynamics but also to quantify the existing decay channels. We determine that ultrafast exciton dissociation occurs in blends and leads to two separate pools of products, namely Coulombically bound charge-transfer (CT) states and unbound (free) charge carriers. The recombination dynamics are analyzed within the framework of a previously reported model for poly(3-hexylthiophene):PCBM (Howard, I. A. et al. *J. Am. Chem. Soc.* 2010, 132, 14866) based on concomitant geminate recombination of CT states and nongeminate recombination of free charge carriers. The results reveal that only ~11% of the initial photoexcitations generate interfacial CT states that recombine exclusively by fast nanosecond geminate recombination and thus do not contribute to the photocurrent, whereas ~89% of excitons create free charge carriers on an ultrafast time scale that then contribute to the extracted photocurrent. Despite the high yield of free charges the power conversion efficiency of devices remains moderate at about 3.0%. This is largely a consequence of the low fill factor of devices. We relate the low fill factor to significant energetic disorder present in the pristine polymer and in the polymer: fullerene blends. In the former we observed a significant spectral relaxation of exciton emission (fluorescence) and in the latter of the polaron-induced ground-state bleaching, implying that the density of states (DOS) for both excitons and charge carriers is significantly broadened by energetic disorder in pristine PCDTBT and in its blend with PCBM. This disorder leads to charge trapping in solar cells, which in turn causes higher carrier concentrations and more significant nongeminate recombination. The nongeminate recombination has a significant impact on the *IV* curves of devices, namely its competition with charge carrier extraction causes a stronger bias dependence of the photocurrent of devices, in turn leading to the poor device fill factor. In addition our results demonstrate the importance of ultrafast free carrier generation and suppression of interfacial CT-state formation and question the applicability of the often used Braun–Onsager model to describe the bias dependence of the photocurrent in polymer: fullerene organic photovoltaic devices.



1. INTRODUCTION

Photovoltaic devices are considered to be one of the most important alternatives to fossil fuels for clean and renewable energy production and to satisfy the world's ever growing energy demand by exploiting a quasi-inexhaustible energy source, the sun. During the last two decades organic semiconductors have

emerged as a new class of photovoltaic materials that promise low-cost and large-area production of organic photovoltaic (OPV) devices using energy-efficient solution-cast techniques

Received: February 28, 2011

Published: May 10, 2011

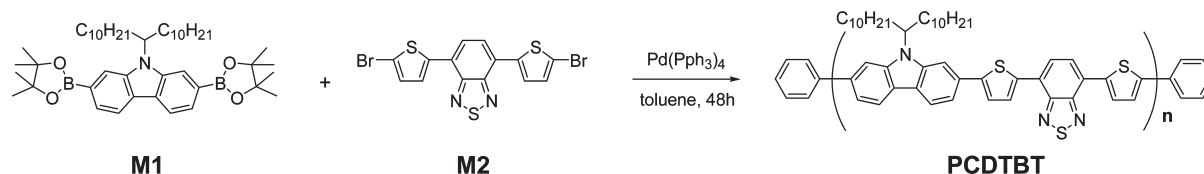
and add unprecedented features such as mechanical flexibility and very low weight, which is of utmost importance for the growing market of mobile electronic devices.¹ In fact organic solar cells based on intimately mixed electron-rich donor polymers and electron-deficient fullerene-based acceptors, commonly referred to as 'bulk heterojunction (BHJ)', have recently demonstrated certified power conversion efficiencies (PCE) exceeding 7–8%.^{2,3} However, the photophysical processes that govern charge generation, transport, and extraction as well as the efficiency-limiting loss channels remain not well understood.⁴ This is partially a consequence of the very complicated interplay between the chemical structure of the individual components, the solid-state morphology of the blend, and the blend photo-physics that finally altogether determine the device efficiency.^{5–7}

It is now widely accepted that in archetypical polymer:fullerene bulk heterojunctions photon absorption leads to the generation of Coulombically bound Frenkel-type excitons, which are the primary photoexcitations in conjugated polymers and small organic molecules.^{8–10} After diffusion to an interface, the exciton is ionized in an ultrafast (<100 fs) process leading to the generation of Coulombically bound charge-transfer (CT) states (also termed bound radical pairs), and free charge carriers (polarons). The ratio of CT states to free charge carriers formed by exciton quenching depends on both the material system and morphology. For efficient photovoltaic operation the ultrafast formation of free carriers is preferred, and although the mechanism for this ultrafast formation of free carriers is unclear, it has been shown to dominate in efficient P3HT:PCBM blends.^{11,12} The effect of interfacial charge transfer states, should they be formed, on photovoltaic efficiency is still debated.^{13–16} Theoretically the CT states could either recombine to the ground state, a process termed geminate recombination, or dissociate into free charge carriers that can be extracted from the blend as photocurrent. The field and temperature dependence of CT-state dissociation (theoretically explored by Onsager, Braun, and Tachiya)^{17–20} have been often invoked to explain the bias dependence of photocurrent. However, recent results in the P3HT:PCBM system suggest the field dependence of the competition between extraction and nongeminate recombination of free carriers determines the field dependence of the photocurrent,^{21,22} calling into question the relevance of field-dependent CT-state splitting in efficient photovoltaic devices. We do note, however, that Lee et al. demonstrated P3HT:PCBM devices exhibit similar internal quantum efficiencies for band gap excitation of Frenkel-type excitons and below band gap direct excitation of CT states,²³ which could imply that what is measured in transient absorption as ultrafast free charge generation could actually very briefly pass through a (hot) charge-transfer state within the ~100 fs instrument response time of the system. What is clear, is that the ratio between what we will continue to term ultrafast generated free charge carriers (with the aforementioned proviso born in mind) and CT states that have been found to geminately recombine on the time scale of approximately a nanosecond in a variety of systems, is an important factor in efficient photovoltaic operation and one that differentiates whether improvement should be sought in improving the separation of charge carriers from the interface by energetic or nanomorphological changes or in their extraction by improvement in mobility or mesoscopic device structure.

In the present work we report direct optical probes of exciton and charge carrier dynamics in a donor–acceptor copolymer, namely poly[N-11''-henicosanyl-2,7-carbazole-*alt*-5,5'-(4',7'-di-2-thienyl-2',1',3'-benzothiadiazole)] (PCDTBT). Copolymers

based on alternating donor–acceptor moieties have recently attracted considerable attention since they in principle can offer better photon harvesting in the lower-energy part of the solar spectrum and/or an increased open-circuit voltage of the devices by fine-tuning of the energy levels of the polymer. PCDTBT attracted our attention because internal quantum efficiencies approaching unity in blends with PCBM have been demonstrated by the Heeger group in conjunction with power conversion efficiencies up to 6.1% upon insertion of optical spacers and in inverted solar cell structures.^{24,25} Earlier work by Leclerc and co-workers on PCDTBT:PCBM photovoltaic devices has demonstrated reproducible efficiencies of more than 3% in simple as-cast device structures, with efficiencies exceeding 5% upon optimizing the light management of the device.^{26,27} Interestingly it was also observed that annealing did not have a positive effect on the device efficiency unlike that typically observed for the prototypic photovoltaic system P3HT:PCBM.²⁸ Recently, Street and co-workers have performed transient photoconductivity measurements on PCDTBT:PCBM devices and concluded that geminate recombination, as can be expected due to the high IQEs, is not at all a significant loss channel in this system.²⁹ Tong et al. have investigated the exciton dynamics in pristine PCDTBT polymer films and charge generation in blends with PC₇₀BM by means of optical probes,³⁰ however, only up to 2 ns, which hampers a clear comparison between geminate and nongeminate recombination and thereby also a direct comparison between CT state and ultrafast free carrier formation. Their analysis is also limited by the fact that the excited-state dynamics were fitted with a sum of exponential functions rather than kinetic equations based on a photophysical model. Hence, the lifetimes reported have no direct physical meaning and only information about the approximate time scale of the processes after the precise excitation fluences used can be gained, making a general comparison problematic. Furthermore, a quantification of the different decay channels occurring on largely varying time scales is also impossible. In a subsequent work the Heeger group studied also the exciton dynamics in pristine PCDTBT polymer films by ultrafast fluorescence upconversion to disentangle the very early excited-state dynamics which occur below 100 fs.³¹ It was suggested that charge carriers are directly generated as primary photoexcitations and collapse into Coulombically bound excitons within the first 100 fs, which is in stark disagreement with the common notion that the primary photoexcitations in conjugated polymers are Frenkel-type excitons. In the present work we report on exciton dynamics in pristine polymer films and charge generation and recombination dynamics covering a dynamic range of 10 orders, i.e., from 100 fs to 1 ms. By studying the entire relevant time scale, we can directly compare geminate (occurring on roughly a few nanoseconds time scale) and nongeminate recombination (occurring, depending on the fluence, on roughly 1 ns to 1 μ s time scales at typical transient absorption pump fluences) processes by studying the charge recombination as a function of initial charge density (i.e., as a function of different excitation fluences). In contrast to previous work, we use our recently introduced analytical model to describe the data and thereby extract the absolute fractions of geminate and nongeminate recombination as well as the relevant rate constants, recombination coefficients, and order of the recombination process. Our results demonstrate that geminate recombination plays a minor role in PCDTBT:PCBM blends and free charge carriers are created without passing through CT states as intermediates, a fact which has recently been demonstrated in P3HT:PCBM

Scheme 1. Synthesis of the Solution-Processable Poly(2,7-carbazole) Derivative PCDTBT



blends, but whose universal validity for high-efficiency polymer: fullerene blends is a matter of ongoing debate.^{4,13} However, we not only quantify the photophysical processes in PCDTBT:PCBM blends by studying the entire relevant time scale but also observe various spectral signatures of significant energetic disorder in the PCDTBT blend not seen in P3HT:PCBM blends by using a broadband probe, which allows us to clearly distinguish between spectral shifts and recombination processes. Having excluded that geminate recombination plays an important role as a loss channel, our experimental results let us conclude that the high disorder leads to higher carrier densities which in turn shift the competition between charge extraction and nongeminate recombination in favor of nongeminate recombination. The increased importance of nongeminate recombination in these devices leads to this recombination playing an increased role in devices under standard operation conditions and explains the reduced fill factor, which is a consequence of the increased bias dependence of the photocurrent. Hence, the investigated devices exhibit only moderate efficiencies not exceeding those obtained from P3HT:PCBM reference cells, despite their higher open-circuit voltage and similar short-circuit current.

2. MATERIAL SYNTHESIS

For the present work a slightly different PCDTBT derivative than has previously been used by most groups was prepared. The material has slightly longer alkyl chains, which provides better solubility in commonly used organic solvents such as toluene and chloroform. The starting materials 2,7-bis(4',4',5',5'-tetramethyl-1',3',2'-dioxaborolan-2'-yl)-N-11''-henicosanylcabazole and 4,7-bis(5-bromo-2-thienyl)-2,1,3-benzothiadiazole used for polymerization were prepared according to a high-yield synthesis previously described in the literature.^{26,32} The dioxaborolan-functionalized carbazole unit (M1) was reacted with the dibromo-functionalized benzothiadiazole (M2) unit under typical Suzuki cross-coupling conditions catalyzed by Pd(PPh₃)₄ in toluene to give PCDTBT as shown in Scheme 1. The resulting polymer was subsequently purified by Soxhlet extraction with hexane, acetone, and methanol. The benzothiadiazole-based poly(2,7-carbazole) was highly soluble in common organic solvents and showed good thermal stability.

3. EXPERIMENTAL SECTION

Tetrakis(triphenylphosphine)palladium(0) (Pd(PPh₃)₄) and tetraethylammonium hydroxide (Et₄NOH, 20% solution) were obtained from Aldrich Chemical Co. and used without further purification. Tetrahydrofuran (THF) was distilled over sodium benzophenone ketyl under nitrogen prior to use. ¹H NMR and ¹³C NMR spectra were recorded with a Varian Oxford 300 MHz NMR spectrometer; chemical shifts are given in ppm with tetramethylsilane used as the internal standard. Mass spectra were taken with a JEOL JMS-AX505WA mass spectrometer.

Synthesis of 2,7-Bis(4',4',5',5'-tetramethyl-1',3',2'-dioxaborolan-2'-yl)-N-11''-henicosanylcabazole. N-11''-Henicosanyl-2,7-dibromocabazole (1.62 g, 2.61 mmol) was dissolved in 30 mL of anhydrous THF in a well-dried round flask under nitrogen atmosphere; 3.6 mL (5.73 mmol) of *n*-butyllithium (1.6 M in hexanes) was added dropwise at −78 °C with stirring for 1 h. After formation of white precipitation, 2-isopropoxy-4,4,5,5-tetramethyl-1,3,2-dioxaborolane (1.3 mL, 6.52 mmol) was added dropwise, and the mixture was allowed to warm to room temperature and stirred for another 6 h. After the reaction, the crude mixture was poured into the water and extracted with dichloromethane. The organic layer was washed with brine (30 mL) and dried over anhydrous magnesium sulfate. The residue was purified by column chromatography to give M1 (1.5 g, 81%) as white powder. ¹H NMR (300 MHz, CDCl₃, ppm): δ 8.59 (br, 1H); 8.40 (br, 1H); 8.19 (d, 1H); 8.15 (t, 2H); 8.09 (d, 1H); 4.50(m, 1H); 2.32 (m, 2H); 1.61 (m, 2H); 1.21 (br, 4H); 1.19–1.15 (br, 28H); 1.03 (br, 24H); 0.88 (t, 6H); EI-Mass: Calculated for C₄₅H₇₃B₂NO₄: 713.57, Found: 713.56

Synthesis of 4,7-Bis(5-bromo-2-thienyl)-2,1,3-benzothiadiazole. ¹H NMR (300 MHz, CDCl₃, ppm): δ 7.84 (d, 2H), 7.82 (s, 2H), 7.19 (d, 2H); ¹³C NMR (75 MHz, CDCl₃, ppm): δ 152.3, 140.7, 130.9, 127.8, 125.5, 125.0; EI-Mass: Calculated for C₁₄H₆Br₂N₂S₃: 455.81, Found: 455.82

Synthesis of Poly[N-11''-henicosanyl-2,7-carbazole-alt-5,5-(4',7'-di-2-thienyl-2',1',3'-benzothiadiazole)] (PCDTBT). A mixture of M1 (0.37 g, 0.524 mmol) and M2 (0.24 g, 0.524 mmol) in 8 mL of anhydrous toluene was degassed two times with N₂. Then, tetrakis(triphenylphosphine)palladium (0.03 g, 0.026 mmol) and 3 mL of 20% Bu₄NOH were added and stirred for 30 min. The mixture was stirred vigorously at reflux for 2 days. After the reaction, the crude product was poured into methanol. The resulting polymer was collected by filtration, and the filtrate was purified by Soxhlet extraction with hexane, acetone, and then methanol. (Yield 76%)

Photovoltaic Devices. For solar-cell preparation ITO-coated glass substrates (Präzisions Glas & Optik GmbH, Germany) were patterned by wet etching and successively cleaned in an ultrasonic bath with different solvents. Between the cleaning steps the samples were dried with nitrogen gas. Prior to spin-coating of the organic films, the substrates were plasma etched for 15 min in argon plasma. After spin-coating of a 20-nm layer of poly(3,4-ethylene-dioxythiophene):poly(styrenesulfonate) (PEDOT:PSS) (Clevios P VP Al 4083, H.C. Stark), the samples were transferred into a nitrogen-filled glovebox and baked for 1 h at 120 °C. For the active layer, PCDTBT and PCBM (Sigma Aldrich) were dissolved separately in chloroform for about 5 h and then mixed in a ratio of 1:2 by weight with a PCDTBT concentration of 5 mg mL^{−1}. The PCBM solution was filtered through a PTFE filter (0.45 μm), then mixed with the PCDTBT solution and spin-cast at 700–2500 rpm for 60 s, producing active-layer thicknesses between 80 and 130 nm. A 100-nm layer of aluminum was subsequently evaporated as a top electrode. For the spectroscopy the active layer was spin-cast onto quartz substrates under conditions similar to those for the solar cells, except that the concentration of PCDTBT in the pristine films was higher with c(PCDTBT) = 10 mg mL^{−1}. For measurements on annealed devices and films, these were heated in the glovebox for 20 min at 120 °C. Solar-cell device characterization was performed inside a nitrogen-filled glovebox employing a solar simulator (K.H.

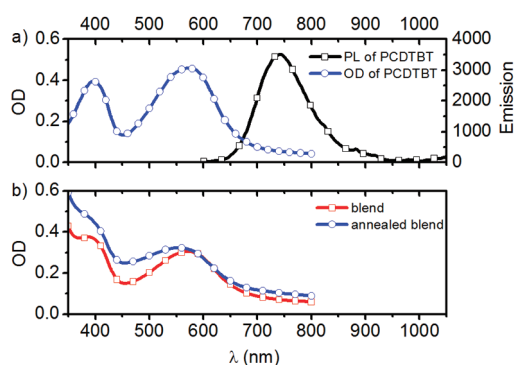


Figure 1. (a) Absorption and emission spectrum of a pristine PCDTBT film ($d \approx 100$ nm). (b) Absorption spectrum of a 1:2 by weight PCDTBT:PCBM blend before and after annealing.

Steuernagel Lichttechnik GmbH, Germany) with a 575 W metal halide lamp combined with a filter system to create a spectrum according to AM1.5G conditions, however, with an intensity of 90 mW cm^{-2} . The current–voltage curves were measured with a Keithley 236 Source-Measure Unit. For external quantum efficiency (EQE) measurements monochromatic light was created with a tungsten–halogen lamp and a TRIAX 180 monochromator between 300 and 800 nm. The light intensity was measured with a calibrated silicon diode leading to a maximum intensity of 0.7 W m^{-2} at 600 nm. EQE measurements were performed in the glovebox at short circuit conditions with a Keithley 236 Source-Measure Unit.

Steady-State Spectroscopy. The absorption measurements were conducted with a Perkin-Elmer Lambda 25 spectrophotometer. Photoluminescence spectra were recorded with a TIDAS 3D fluorescence spectrometer. To determine the layer thickness of the films a Tencor P10 surface profilometer was used.

Quasi-steady-state Spectroscopy. Quasi-steady-state photoinduced absorption spectroscopy (PIA) was performed with a pump–probe setup consisting of a 100 W tungsten-halogen lamp with a LOT-Oriel Omni- λ 300 monochromator as the probe and a Newport LED (LED-527-HP) working at 524 nm with 100 mW cm^{-2} used as a pump. The samples were placed in a nitrogen-cooled optical cryostat (Oxford Instruments Optistat CF) at 80 K in helium atmosphere. The transmitted light was dispersed by a second identical monochromator and then detected by a photodetector. For measurements in the wavelength range from 500 to 1100 nm, an amplified silicon photodetector (Thorlabs PDA 100A) was employed, which was replaced by an amplified germanium detector (Thorlabs PDA 50B) for the wavelength range from 900 to 1800 nm. The pump light was chopped at 317 Hz to induce changes in the transmission ΔT , which were measured by using a lock-in amplifier (EG&G Princeton Applied Research model 5210). To calculate $\Delta T/T$, the transmission was recorded prior to the PIA measurement and corrected for photoluminescence.

Time-Resolved Fluorescence. Time-resolved photoluminescence (TR-PL) spectra were measured with a C4742 Hamamatsu streak camera system. Samples were excited with the frequency doubled output from a mode-locked Ti:Sa oscillator (Coherent Mira 900 Duo) with a pulse width of 100 fs at 400 nm.

Transient Absorption Spectroscopy. Transient absorption (TA) measurements were performed with a home-built pump–probe setup. To measure in the time range of 1–4 ns with a resolution of ~ 100 fs, the output of a commercial titanium:sapphire amplifier (Coherent LIBRA HE, 3.5 mJ, 1 kHz, 100 fs) was split with one portion used to generate a 532 nm excitation pulse using a home-built two-stage narrowband non-collinear optical parametric amplifier (NOPA) and another used to generate a 1300 nm seed pulse (output of an optical

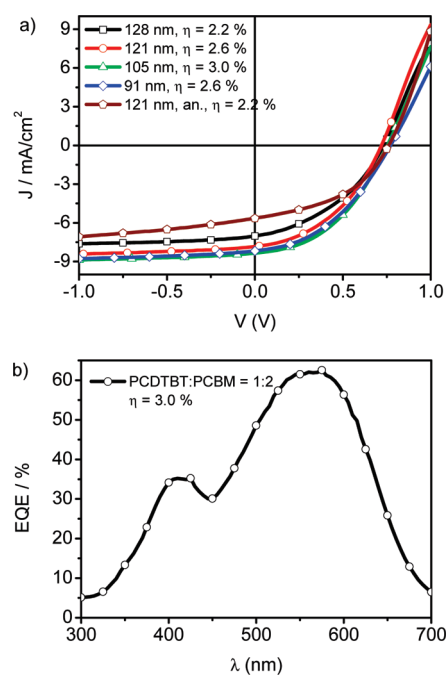


Figure 2. (a) The current–voltage (J – V) characteristics of BHJ solar cells made from 1:2 by weight PCDTBT:PCBM blends for different active layer thickness. η is the power conversion efficiency under solar illumination of 90 mW cm^{-2} . The efficiency is found to decrease upon annealing. (b) External quantum efficiency of the solar cell with a 105-nm active layer thickness measured at short-circuit conditions.

parametric amplifier (Coherent OPerA Solo)) for white-light generation in the visible and NIR in a c-cut 3 mm thick sapphire window. The variable delay of up to 4 ns between pump and probe was introduced by a broadband retroreflector mounted on a mechanical delay stage. Only reflective elements were used to guide the probe beam to the sample to minimize chirp. The excitation pulse was chopped at 500 Hz, while the white light pulses were dispersed onto a linear photodiode array which was read out at 1 kHz. Adjacent diode readings corresponding to the transmission of the sample after an excitation pulse and without an excitation pulse were used to calculate $\Delta T/T$. For measuring in the time range of 1 ns to 1 ms with a resolution of 600 ps, the excitation pulse was provided by an actively Q-switched Nd:YVO₄ laser (AOT Ltd. MOPA) at 532 nm. The delay between pump and probe in this case was controlled by an electronic delay generator (Stanford Research Systems DG535). TA measurements were performed at room temperature under dynamic vacuum at pressures $< 10^{-5}$ mbar.

4. EXPERIMENTAL RESULTS

4.1. Photovoltaic Performance. Figure 1a shows the steady-state absorption spectra of a pristine PCDTBT film and an as-cast and annealed 1:2 by weight PCDTBT:PCBM blend. We note that the PCDTBT derivative used in our study has a longer alkyl chain attached to the nitrogen of the carbazole comonomer (11'-henicosanyl instead of 9'-heptadecanyl) than the polymer used in previous studies, which provides better solubility of the polymer in organic solvents commonly used for thin film preparation. However, in agreement with previous reports we observe two distinct absorption bands from the polymer backbone peaking at 397 and 572 nm. The lower-energy absorption band has previously been assigned to the π – π^* -transition of the first excited singlet state (S_1) of the conjugated backbone, while

Table 1. Photovoltaic Parameters of PCDTBT:PCBM (1:2) Solar Cells with Varying Active Layer Thickness under Solar Illumination of 90 mW cm⁻²

device	active layer [nm]	V _{oc} [V]	J _{sc} [mA cm ⁻²]	FF	PCE [%]
1	128	0.73	-7.02	0.40	2.2
2	121	0.72	-7.84	0.42	2.6
3	105	0.75	-8.35	0.43	3.0
4	91	0.77	-8.17	0.41	2.6
5	121 annealed	0.76	-5.65	0.44	2.2

the higher-energy absorption band has been attributed to the π - π^* -transition into the second excited singlet state (S_2).³¹ Excitation into both the lower-energy band of the absorption spectrum at 532 nm and the higher-energy band at 400 nm leads to a broad and unstructured emission between 620 and 940 nm, peaking at 742 nm in the steady-state spectrum. In blends with PCBM the energetically lower absorption peak of PCDTBT is still visible, whereas the band at 400 nm is superimposed by the fullerene absorption. We observe that annealing has only a limited impact on the absorption of the blend, unlike that observed for regioregular P3HT:PCBM blends.

Figure 2a shows the J - V characteristics of PCDTBT:PCBM (1:2) solar cells under solar illumination of 90 mW cm⁻². The best power conversion efficiency (PCE) of \sim 3% was obtained for an active layer thickness of 105 nm. Typical photovoltaic parameters obtained from PCDTBT:PCBM(1:2) solar cells are shown in Table 1.

The best device showed a moderate fill factor (FF) of 0.43 (lower than the 0.6 typically observed for P3HT:PCBM)²² with an open circuit voltage (V_{oc}) of 0.75 V and a short circuit current density (J_{sc}) of 8.35 mA cm⁻². A decrease of the device efficiency upon prolonged annealing can be observed in line with previous reports.²⁸ The short circuit current of the solar cells was found to depend linearly on the illumination intensity (see Supporting Information), indicating that at short circuit conditions the total fraction of recombination reducing the photocurrent (i.e., the sum of geminate and nongeminate recombination) is constant in the entire intensity range measured. As we consider further, the effects of nongeminate recombination may, however, increase as the internal field is reduced and the open-circuit voltage is approached. The external quantum efficiency for the best devices is shown in Figure 2b. The EQE exhibits two peaks coinciding with the absorption maxima of the blend. The EQE approaches 63% at the energetically lower peak, i.e. at the absorption maximum of the polymer. At around 400 nm the EQE is lower and around 35%, despite the higher absorption of the blend at this wavelength for reasons still not entirely understood. However, this seems to indicate that, as observed previously in the P3HT:PCBM system, quenching of excitons created on PCBM is less complete than quenching of excitons created on the polymer.³³

4.2. Exciton Dynamics in Pristine PCDTBT Films. Figure 3 shows a contour plot of the time-resolved (0–2 ns) photoluminescence (PL) of a pristine PCDTBT polymer film at room temperature measured by a Streak Camera after excitation with the frequency doubled output of a titanium:sapphire femtosecond oscillator (400 nm, \sim 100 fs). The PL progressively red-shifts, indicating relaxation of excitons in the density of states. The relaxation is significant, corresponding to a shift in energy of about 70 meV that is completed on the time scale of approximately 1 ns (see Supporting Information). Simulations have

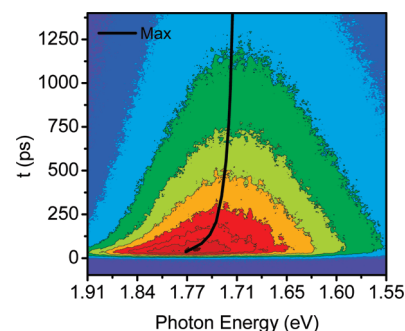


Figure 3. Temporal evolution (ps–ns) of the photoluminescence of pristine PCDTBT films as observed by the Streak Camera technique after excitation with a femtosecond laser pulse. The solid line shows the evolution of the peak position of a Gaussian line shape fit to the spectrum at each time delay.

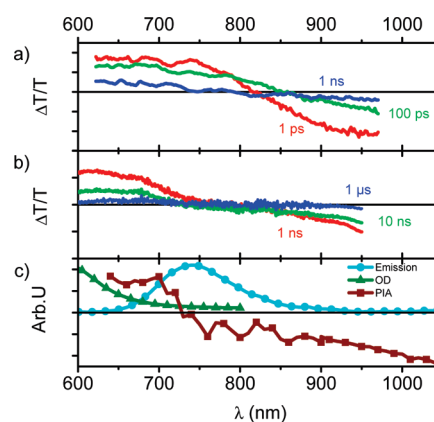


Figure 4. Transient absorption spectra for pristine PCDTBT films between 1 ps and 4.5 ns (panel a) and 1 ns to 4.5 μ s (panel b). The short-time pump fluence was 7.1 μ J cm⁻², and the long-time pump fluence was 37 μ J cm⁻². (Panel c) Steady-state absorption and photoluminescence spectra and the quasi-steady-state PIA spectrum of pristine PCDTBT.

demonstrated that disorder on such a scale significantly influences device performance.³⁴ We will see later that this large broadening due to significant energetic disorder also plays a role in the kinetics of charge carriers formed in blends.

Figure 4 shows the short-time (fs–ns) and long-time (ns– μ s) transient absorption spectra of the same pristine polymer film as well as the steady-state absorption, PL and PIA spectrum for comparison. Let us first discuss the short-time TA spectra shown in the upper panel of Figure 4. The early time spectra consist of a positive TA signal extending to shorter wavelengths, a time-dependent zero-crossing, and a broad negative TA signal extending to longer wavelengths than detected. The positive TA feature can be attributed to a superposition of the ground-state bleaching (GSB) and stimulated emission (SE) of the polymer, since in this spectral region the absorption and fluorescence of the polymer are typically observed. The latter can be attributed to photo-induced absorption mostly from singlet excitons. The SE red-shifts with time in the same fashion observed in the time-resolved fluorescence measurement. The decay of the SE signal is pump intensity-dependent, indicating that higher-order processes occur at the higher-excitation fluences. However, at the two lowest-pump fluences the SE dynamics converge (see Figure 5) and can

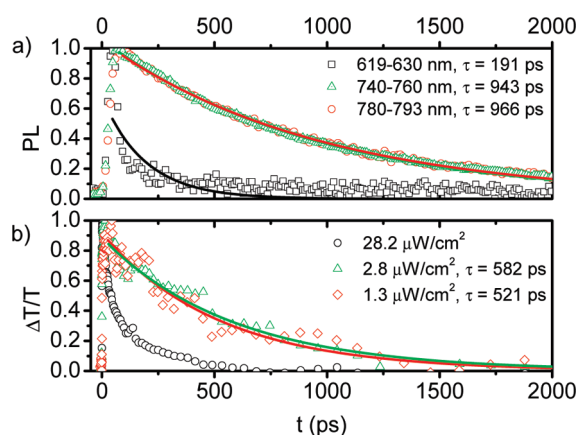


Figure 5. (a) Decay of the PL in pristine PCDTBT films obtained from Streak Camera measurements. The solid lines correspond to single exponential fits. The decay kinetics are affected by significant spectral relaxation. The decay in the lower-energy tail (i.e. longer-wavelength region of the fluorescence) is quasi-single exponential with a lifetime of ~ 966 ps, whereas that at shorter wavelength is a stretched exponential caused by fast energy transfer away from the high-energy states. The black line corresponds to a single-exponential decay but fails to fit the data. (b) Decay of the SE in pristine PCDTBT film averaged between 740 and 760 nm obtained from transient absorption measurements. The kinetics are fluence dependent. At the two lowest fluences measured, a single exponential fit to the data yields a SE lifetime between 500 and 600 ps.

be reasonably described by a single exponential with an inverse rate of ~ 600 ps. Comparing this value to the rates inferred from the time-resolved PL experiments, see Figure 5, demonstrates that very low excitation densities are needed in pristine PCDTBT to completely avoid bimolecular effects. This could be caused by the disorder effectively funneling excitons toward lower-energy sites increasing the local population at these low-energy areas and thereby promoting exciton–exciton interactions.

An isosbestic point (which indicates the presence of only a single excited species) is not observed in the short-delay spectra shown in the upper panel of Figure 4. Instead, the zero-crossing is time dependent and blue-shifts at longer delay times, indicating a second population is present, which is much longer-lived than the initial photoexcitations. The long-delay TA spectra shown in the middle panel of Figure 4 support this observation. Here we observe a clear isosbestic point between GSB and PA and no more SE pointing to the presence of a nonemissive species. Furthermore, the long-delay TA spectra are virtually identical to the quasi-steady-state PIA spectra shown in the bottom panel of Figure 4, which is expected, since the latter exclusively monitors long-lived excited states such as triplet states and charge carriers. We note at this point that the origin of the long-lived signal cannot be uniquely identified from the spectra, since it may be caused by triplet states or charge carriers generated in the pristine polymer. However, the decay dynamics of triplets and charge carriers are typically largely different, with triplets returning to the ground state in a monomolecular process^{35,36} featuring a defined excited-state lifetime expected to be hundreds of nanoseconds to several microseconds and charge carriers typically following bimolecular or power-law recombination dynamics.³⁷ In fact, for the signal present in the long-delay TA spectra we observe a single-exponential decay (see Supporting Information) with a lifetime on the order of 2–3 μ s and therefore assign this

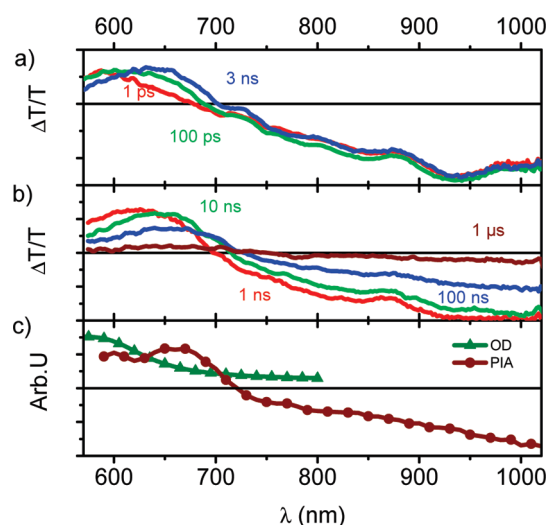


Figure 6. Transient absorption spectra of PCDTBT:PCBM(1:2) between 1 ps and 3 ns (panel a) and 1 ns and 4.5 μ s (panel b) pumped at $23.7 \mu\text{J cm}^{-2}$ and $25.7 \mu\text{J cm}^{-2}$, respectively. Panel c shows the ground-state absorption and PIA spectra of the blend.

signal to triplet states. It is noteworthy to mention the similarity of the pristine PCDTBT photophysics to the processes recently reported for pristine films of regiorandom poly(3-hexylthiophene), where intersystem crossing from the singlet to the triplet state was observed by us and others.^{11,38} To sum up, we note that pristine PCDTBT exhibits typical features of an energetically disordered conjugated polymer with a broad density of states, allowing for pronounced spectral relaxation of excited states. A fraction of the primary photoexcitations undergoes intersystem crossing to the triplet state. However, the absolute value of triplet state formation remains unknown, since the cross sections of the individual excited states have not been determined.

4.3. Photophysics of PCDTBT:PCBM Blends. **4.3.1. Charge Generation and Relaxation.** In Figure 6 we present results of transient absorption experiments on as-cast PCDTBT:PCBM (1:2) blends. Panel a shows the time range from 1 ps to 3 ns, and panel b longer delay times ranging from 1 ns up to 5 μ s. In both time frames three distinct features can be observed, a positive signal from 550 to 700 nm, a time-dependent zero-crossing, and a broad negative signal between 700 and 1100 nm (upper limit of our silicon detector). Comparing panels a and b (Figure 6) with the steady-state measurements shown in panel c reveals that the positive change in transmission at smaller wavelengths is caused by the bleaching of the ground state, as it is coincident with the absorption spectrum in this wavelength range shown in panel c (Figure 6). The blue curve in panel c is obtained from PIA spectroscopy and indicates the existence of long-lived excited states. This signal is attributed to charge carriers because in the blend singlet excitons are quenched by electron transfer from the polymer to the PCBM with a rate much faster than that of triplet formation, so that very few triplets can be expected, if formed at all. The extended near-infrared wavelength range of the PIA also suggests that the PA of charge carriers expands further into the infrared at least up to 1800 nm which is the detection limit of our germanium detector (see Supporting Information). The absence of a positive signal between 700 and 850 nm in the short-delay TA measurements indicates that the SE, which could be observed

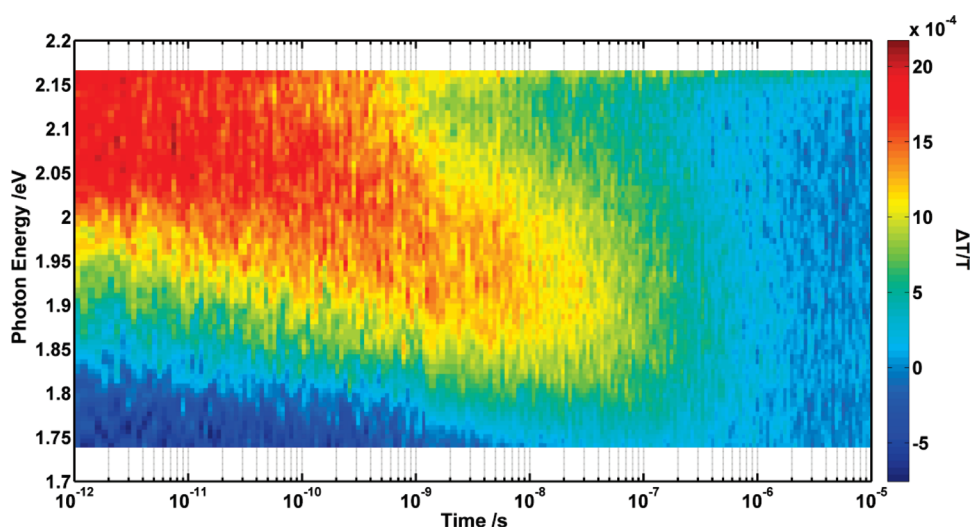


Figure 7. Spectral relaxation of the ground-state bleaching in PCDTBT:PCBM blend films after photoexcitation. Note that the bleaching is caused by charge carriers that relax in the blend film. The image is a straight combination of the short-delay (ps–ns) and the long delay (ns–ms) transient absorption data without any additional scaling parameter.

in the pristine polymer film, is strongly quenched due to (ultra)fast electron transfer from PCDTBT to PCBM, as expected for intimately mixed photovoltaic blends. We also note that the initial signal intensity scales linearly with the pump fluence (see Supporting Information) which shows that nonlinear processes caused by the high excitation fluence are virtually absent in the blend in contrast to the pristine polymer films, where an intensity dependence of the decay dynamics has been observed. This is a consequence of the ultrafast charge transfer process, which effectively suppresses exciton–exciton annihilation or exciton–charge annihilation, which can be observed, if excitons are not instantaneously quenched, as recently shown by us for annealed P3HT:PCBM blends.¹¹ In the region of the PA the signal intensity is almost constant over the entire time range of 3 ns for the pump fluence shown. At smaller wavelengths, where the bleaching is dominant, the signal similarly shows almost no decay, but interestingly does exhibit a spectral relaxation of about 80 meV during the first 3 ns. This relaxation of the ground-state bleaching, indicating that the hole polarons on the polymer shift to lower and lower energy sites, continues up to ~ 150 ns as can be deduced from the long delay measurements, shown in panel b (Figure 6)). The zero-crossing finally coincides with the spectral position obtained from the quasi-steady-state PIA, shown in panel c (Figure 6)). The long-lived signal can be ascribed to charge carriers generated in the blend that recombine with a density dependent rate that at the fluences typical for transient absorption leads to decays varying from nanoseconds to microseconds, depending on the excitation intensity. The long time scale significant relaxation of these hole polarons is rather unusual for polymer:PCBM blends and has not yet been reported. One reason may be that the relevant time range from 1 ns to several hundred nanoseconds is rarely observed in transient absorption experiments to present. We further emphasize that only a broadband spectral detection of the transient absorption signals in the relevant time scale allows observing the relaxation process, which could easily be misinterpreted as a decay process if single-wavelength detection schemes were employed. Figure 7 displays the entire relaxation in a matrix image of the transient absorption data. The peak of the ground-state bleaching relaxes

from approximately 2.1 eV at short time to 1.9 eV after ~ 150 ns. This relaxation of ~ 200 meV is surprisingly large and clearly indicates that energetic disorder significantly affects the charge carriers on the PCDTBT chains. In fact, the observed shift is even larger than observed for the excitons in pristine PCDTBT, suggesting that, if disorder has a similar broadening effect on the DOS for excitons and holes, disorder may be enhanced in the blend film most probably caused by the large fraction of PCBM molecules present in the blend. The observed spectral relaxation also indicates that the free charge carriers created immediately after photoexcitation are initially hot and tend to relax to states of lower energy within the DOS. This can be understood in terms of diffusion away from a rather disordered interfacial region, which intrinsically is of higher energy, into the bulk of the polymer, which provides better order and thus states of lower energy.

4.3.2. Charge Carrier Recombination Dynamics. In the following we analyze more closely the decay dynamics of the TA signals of PCDTBT:PCBM and find that an analytical model developed to describe charge recombination in prototypic P3HT:PCBM blends¹¹ also accurately describes the behavior of the current system. From this analytical model we evaluate (i) the branching ratio of geminate versus nongeminate recombination (which is equal to the branching ratio between CT and ultrafast free charge generation), (ii) the geminate recombination rate constant, (iii) the nongeminate recombination coefficient, and (iv) the order of nongeminate recombination.

Since the GSB is obscured by spectral relaxation as described above, the dynamics are strongly wavelength dependent. Therefore, in order to purely track the kinetics of the charge population we consider instead the red part of the PA signal averaged from 865 to 1000 nm which is undisturbed by spectral relaxation. The short-time decay dynamics of the PA are intensity dependent; however, at the lowest-excitation intensities used in our TA experiments the dynamics obtained after excitation at 532 nm converge and level off at $\sim 90\%$ of the initial signal intensity after about 3 ns (see Supporting Information). A monoexponential fit to the early time 10% decay of this reveals a decay rate of $k = 4.5 \times 10^8 \text{ s}^{-1}$, corresponding to a lifetime of ~ 2.2 ns, which we attribute to intensity-independent geminate recombination of

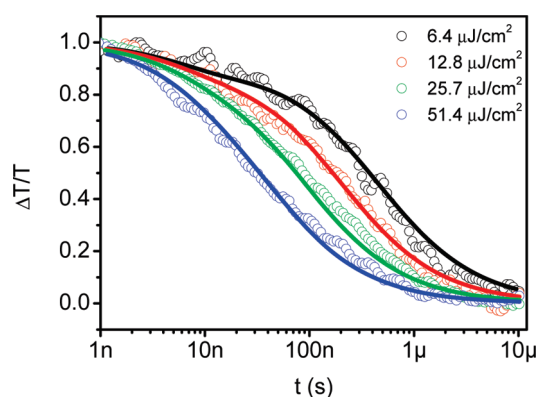


Figure 8. Normalized decay dynamics (ns–ms setup) of the charge-induced absorption between 865 and 1000 nm for different pump fluences. Note the faster decay at higher fluences due to accelerated nongeminate recombination of free charge carriers. The solid lines represent fits to our analytical model of charge recombination.

interfacial CT states. Interestingly, the decay rate and thus the CT-state lifetime is very similar to that observed previously in regiorandom P3HT:PCBM blends, as-cast (unannealed) regioregular P3HT:PCBM blends,^{11,12} and also some polymer:polymer blends,³⁹ indicating that nanosecond CT-state recombination is not unusual, and may even be rather general in photovoltaic blends. The short time decay dynamics are also unaffected by annealing of the samples, indicating that the photophysical processes do not significantly change when the blends are annealed in line with the insignificant impact of annealing on the device efficiency (see Supporting Information).

In Figure 8 we present the decay traces of the PA signal obtained from long-delay TA measurements at pump energies between $6.4 \mu\text{J cm}^{-2}$ and $51.4 \mu\text{J cm}^{-2}$. The decay profiles are intensity-dependent, indicating nongeminate recombination occurs in the blend on a time scale of several nanoseconds to tenths of microseconds. The solid lines shown in Figure 8 present fits according to a recently suggested model for charge recombination, which we briefly introduce in the following. The key aspect of the model is that dissociation of the initially formed strongly bound Frenkel-type singlet excitons leads to two population pools, one being interfacial charge-transfer (CT) states and the other one free charge carriers. The ultrafast exciton dissociation, i.e. the formation of CT states and free charge carriers, is not resolved in our experiment due to the limited instrument response time (~ 100 fs), and thus only the decay of each species is considered. The rate equations describing the population dynamics in the system are shown in eqs 1, 2, and 3.

$$\frac{dCT}{dt} = -k_{CT \rightarrow GS}CT \quad (1)$$

$$\frac{d(SSC)}{dt} = -\gamma SSC^{\lambda+1} \quad (2)$$

$$\frac{dGS}{dt} = k_{CT \rightarrow GS}CT + \gamma SSC^{\lambda+1} \quad (3)$$

The bound charge carriers (CT states) decay monomolecularly to the ground state (GS) with a decay rate $k_{CT \rightarrow GS}$. The spatially separated (free) charge carriers (SSC) decay with the recombination rate γ and the recombination order of λ . Therefore, the ground state is populated via two decay channels, either from

interfacial CT states or from nongeminate recombination of free charge carriers. The solution of the system of differential equations is presented in eqs 4, 5, and 6

$$CT(t) = N_0(1-f)\exp(-k_{CT \rightarrow GS}t) \quad (4)$$

$$SSC(t) = (\lambda\gamma t + (fN_0)^{-\lambda})^{-1/\lambda} \quad (5)$$

$$GS(t) = N_0(1-f)(1 - [\exp(-k_{CT \rightarrow GS}t)]) + N_0f - (\lambda\gamma t + (fN_0)^{-\lambda})^{-1/\lambda} \quad (6)$$

where N_0 is the initial excited state density and f the fraction of nongeminate recombination.

The solution of the rate equations is used to globally fit the recombination dynamics at all the excitation intensities measured. As described above we used the spectral region of the charge-induced absorption to measure the total population of charge carriers and assumed that the cross sections of a charge in a CT state and a free charge are the same. The initial excited-state densities are calculated from the excitation pump fluence used to excite the blends, the blend film thickness, and its optical density at the excitation wavelength. The initial excited-state densities are the only fixed parameters of the fitting procedure. All other parameters are shared among the whole set of intensity-dependent dynamics. We found that the data can be well described by our model as can be seen in Figure 8. We also checked whether a fit based exclusively on nongeminate recombination (i.e., $f = 1$) could adequately reproduce the data, which would point to the absence of fast geminate recombination processes. However, the fit failed to reproduce the data and led to significantly larger deviations from the experimental data. The fitting parameters obtained from a global fit of the entire data set are summarized in Table 2. The model allows several details of the generation and recombination processes to be extracted. Most importantly, we can determine the branching ratio of geminate versus nongeminate recombination which also tells us the branching ratio between ultrafast free charge carrier and CT-state formation. In PCDTBT:PCBM blends we find $\sim 89\%$ nongeminate recombination (ultrafast free carrier formation) and $\sim 11\%$ geminate recombination (CT state formation), implying that only a small fraction of charge carriers are lost to geminate recombination of CT states and the majority can in principle be extracted as photocurrent. From the model we also obtain the order of the recombination process, which is found to be 2.16 and thus close to 2.0, indicating nongeminate recombination in PCDTBT:PCBM follows to a great extent typical three-dimensional Langevin-type recombination as can be expected for an intimately mixed polymer:fullerene blend. The fact that the order is slightly higher than 2 is typically explained by the density dependence of the carrier mobility further increasing the dependence of the rate of recombination on carrier density. In comparison to the single-exponential fits to the 10% decay in the short delay data we obtain a rate constant of $1.8 \times 10^8 \text{ s}^{-1}$, i.e. an inverse rate of 5.6 ns, for the geminate recombination from the global fit to the long delay data. This further supports our previous finding on P3HT:PCBM that interfacial geminate recombination in photovoltaic systems is indeed on the order of a few nanoseconds, which thus appears to be of a more general validity for polymer:fullerene systems.

Table 2. Parameters along with Standard Deviation Extracted from the Global Fit to the Long Delay TA Measurements

parameter	PCDTBT:PCBM	rr-P3HT:PCBM (as-cast) ^a	rr-P3HT:PCBM (annealed) ^a
$1 - f$ (geminate recombination)	0.11 ± 0.01	0.32 ± 0.01	0.15 ± 0.01
f (nongeminate recombination)	0.89 ± 0.01	0.68 ± 0.01	0.85 ± 0.01
k 1/s (geminate recombination rate)	$(1.8 \pm 0.2) \times 10^8$	$(4.9 \pm 0.2) \times 10^8$	$(2.5 \pm 0.2) \times 10^8$
$\lambda + 1$ (order of nongeminate decay)	2.16 ± 0.01	2.18 ± 0.01	2.45 ± 0.01
γ (cm ³) ² s ⁻¹ (nongeminate decay constant)	$(5 \pm 1) \times 10^{-15}$	$(2.3 \pm 0.5) \times 10^{-15}$	$(1.9 \pm 0.3) \times 10^{-20}$
γ_{eff} cm ³ s ⁻¹ (effective $\lambda = 2$ bimolecular decay constant at a charge density of 5×10^{15} cm ⁻³ for direct comparison with literature values)	1.7×10^{-12}	1.5×10^{-12}	1.3×10^{-12}

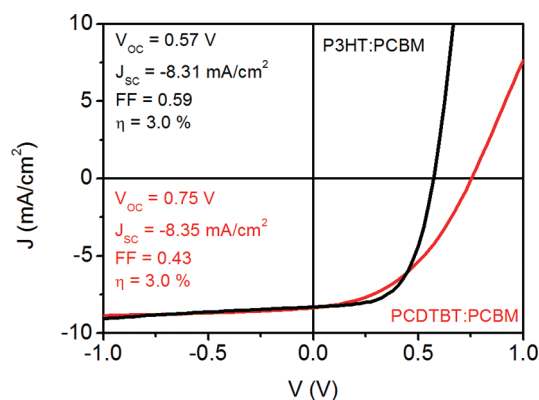
^a Taken from ref 11.

Figure 9. Comparison of the current–voltage characteristics and photovoltaic parameters of optimized regioregular P3HT:PCBM and PCDTBT:PCBM bulk heterojunction organic solar cells. The short-circuit currents are similar, while the increased V_{OC} of the latter material system is offset by a reduced fill factor resulting in very similar device efficiencies.

5. DISCUSSION

Figure 9 compares the current voltage characteristics of a PCDTBT:PCBM solar cell to that of a regioregular P3HT:PCBM solar cell, whose fabrication is described elsewhere.²² Both cells were measured under equal illumination conditions and had similar optical densities. The short-circuit currents of the cells are almost identical, while the higher open-circuit voltage of the PCDTBT cell is offset by a poor fill factor leading to overall similar power conversion efficiencies. The fill factor of a solar cell is determined by its dark current, photocurrent, and their dependence on voltage. For typical dark currents (see Supporting Information) a large fill factor (>0.6) indicates little voltage dependence of the photocurrent while a small fill factor (<0.4) indicates significant voltage dependence of the photocurrent. The voltage dependence of the photocurrent can in principle have its origin in a field-dependent charge generation efficiency (field dependent splitting of CT states) and/or a field-dependent collection efficiency (field dependent competition between charge extraction and nongeminate recombination). In fact, the origin of the voltage dependence of the photocurrent is one of the most controversially discussed issues in the OPV community, as its understanding is of utmost importance, since it is directly related to the mechanism of charge carrier generation. Thus, any information about the early time charge generation and recombination processes of relevant donor:acceptor systems is very

valuable and until now rarely reported in the literature, since the intermediate time range between 1 ns and 1 μ s is experimentally difficult to observe. In the previous section we found that in the absence of field (i.e., under open-circuit conditions) only 11% of the quenched excitons form CT states. This is far too small a fraction of the entire population for a bias dependence of the CT state separation to account for the large change in photocurrent with voltage (to obtain this low fill factor the change of current with bias is much greater than 11% of the short circuit current). We therefore assert that the role of bias-dependent CT state separation cannot significantly contribute to the bias dependence of the photocurrent, which is supported by the recent work of Durrant and co-workers which shows that the field-dependence of the charge-generation efficiency in a prototypic low-bandgap polymer:fullerene photovoltaic device is negligible.⁴⁰ Furthermore, by going to low temperatures to lower the carrier mobility in P3HT:PCBM devices, we have previously shown that the increased bias dependence of the photocurrent (and therefore decreased fill factors) can be entirely explained by the higher charge-carrier densities causing bimolecular recombination to start competing with charge extraction and the bias dependence of this competition causing the bias dependence of the fill factor.²² We therefore state that the primary limitation of the fill factor in the investigated PCDTBT:PCBM solar cells is the bias-dependent collection efficiency caused by the competition between nongeminate recombination and charge extraction rather than a field-dependent CT-state splitting as has often been suggested for related polymer:fullerene systems.^{13,41} The reduction of the fill factor caused by this mechanism is more significant in the case of PCDTBT:PCBM than in P3HT:PCBM blends under standard operation conditions because the large energetic disorder of the PCDTBT creates a large population of low-energy polarons that have a limited mobility and therefore increase the carrier concentration in the device, possibly also leading to space-charge effects. This in turn leads to an increased rate of recombination that is more competitive with the rate of charge extraction. This view of the impact of energetic disorder on the recombination dynamics is qualitatively consistent with the recent suggestion of the impact of trap-assisted recombination (Shockley–Read–Hall (SRH) recombination) in PCDTBT:PCBM blends by Street and co-workers.⁴² In a very recent work Cowan et al. have extended this concept and proposed that high charge carrier trap densities should lead to a decrease of the fill factor,⁴³ which our measurements experimentally corroborate in the model system herein reported. It appears that the recombination dynamics can be interpreted in the framework of the well-established Gaussian disorder model (GDM), which relies on

energetic and positional disorder as the main parameters which influence the photophysics of conjugated materials. Within the framework of the GDM a charge carrier, which has been generated at a random site within the DOS, is expected to relax toward transport sites of lower energy, until it reaches its thermal equilibrium energy. From there it can be thermally excited toward transport sites of higher energy, which facilitate charge transport.^{44–46} The relaxation is pronounced in systems, which exhibit a large energetic disorder, as is the case for the investigated PCDTBT:PCBM. A significant energetic disorder typically leads to lower charge carrier mobilities than observed for materials which have a lower energetic disorder.^{46,47} The latter has been reported recently by us for the P3HT:PCBM reference system, which was shown to exhibit a comparably small energetic disorder of $\sigma = 40$ meV.⁴⁸ Thus, it is obvious from our experimental data that the present PCDTBT:PCBM system suffers from a rather broad density of states as indicated by the significant spectral shifts observed during exciton relaxation and charge carrier migration.

A straightforward consequence of the observed nanosecond geminate recombination, which we have previously shown for P3HT:PCBM and herein extend to PCDTBT:PCBM, is the breakdown of the Braun–Onsager model to explain the field-dependent photocurrents in these systems, which is in contradiction to models previously presented by Deibel and co-workers. In fact, much longer lifetimes of CT states than are directly monitored by optical spectroscopy, typically in the range of hundreds of nanoseconds or even microseconds, are required to satisfactorily reproduce the experimentally observed *IV*-curves, if a Braun–Onsager-type splitting of CT states is used to describe free carrier generation and the bias dependence of the photocurrent.^{41,49–53} Therefore, we believe that ultrafast, sub-picosecond free carrier generation is a general feature of efficient polymer:fullerene photovoltaic systems that is strongly related to both energetic considerations and to the interfacial morphology of the blend. However, even if geminate recombination can be efficiently suppressed and the generation of free charge carriers approaches unity as found for the present case of PCDTBT:PCBM, other efficiency-limiting processes such as nongeminate recombination due to limited charge transport have to be overcome. We suggest that developing a further understanding of the pathways of nongeminate recombination is important to allow new material systems to reach the high fill factors achieved by P3HT:PCBM. For example the question of whether the high fill factor of P3HT:PCBM is simply a consequence of lower carrier densities in the device due to better transport, or whether the partition into more crystalline and amorphous regions allows higher carrier densities to be sustained without increasing the rate of nongeminate recombination has significant bearing on new material design and device engineering.

6. CONCLUSION

Using broadband pump–probe spectroscopy over the entire relevant time range of charge generation and recombination, we show that fast dissociation of the primary photoexcitations in as-cast PCDTBT:PCBM blends leads to the generation of free charge carriers and Coulombically bound interfacial charge-transfer states with a branching ratio of 89% free charge carriers to 11% CT states. The latter recombine monomolecularly to the ground state with a lifetime of about 2.5 ns and thus cannot contribute to the photocurrent. In fact, nanosecond time scale

geminate recombination previously also demonstrated in P3HT:PCBM, appears to be a general phenomenon in polymer:fullerene blends as indicated by our present results, which calls into question the validity of models that describe the bias dependence of the photocurrent based on field-dependent Onsager–Braun-type separation of CT states that invoke CT state lifetimes longer than hundreds of nanoseconds. We note also that a field-dependent separation of the 11% of CT states could not make a large enough contribution to account for the field dependence of the experimentally observed photocurrent. We find that the large fraction of free charge carriers generated in an ultrafast process after photoexcitation recombines predominantly nongeminately on the time scale of nanoseconds to microseconds. In an operating PV device, these free charge carriers can be extracted almost quantitatively at short-circuit. However, at lower internal fields, i.e. in the typical operating range of the organic solar cell, the increased carrier density shifts the competition between carrier extraction and nongeminate recombination in favor of nongeminate recombination, which leads to a strong field dependence of the photocurrent that explains the poor fill factor of the device. This suggests that further optimization of this system should focus on increasing the rate of charge extraction, potentially by decreasing the energetic broadening of transport sites of the polymer in solid state. Also, determining the mechanism that reduces the EQE in spectral regions where the PCBM absorbs remains an open question with significant implications for the device performance.

■ ASSOCIATED CONTENT

S Supporting Information. Further information about the dependence of the short circuit photocurrent on illumination intensity, spectral relaxation of the PL, the triplet decay dynamics of pristine PCDTBT, PIA measurements of pristine PCDTBT, short delay TAS measurements of PCDTBT:PCBM, and *IV*-curves together with the dark current of PCDTBT:PCBM solar cells. This material is available free of charge via the Internet at <http://pubs.acs.org>

■ AUTHOR INFORMATION

Corresponding Author

laquai@mpip-mainz.mpg.de; ian.howard@mpip-mainz.mpg.de; kslee@hnu.kr

■ ACKNOWLEDGMENT

This work is part of the International Research Training Group IRTG 1404 “Self-organized Materials for Optoelectronics” between Germany and Korea funded by the Deutsche Forschungsgemeinschaft (DFG). I.A.H. acknowledges a post-doctoral fellowship of the Alexander von Humboldt Foundation. R.M. and M.M. thank the Max Planck Graduate Center (MPGC) for financial support. F.L. acknowledges support from the Max Planck Society in the framework of the Max Planck Research Group funding scheme. K.S.L. also acknowledges funding of this work from Midcareer Researcher Program through NRF grant funded by the MEST (No. 2010-0000499) and the Asian Office of Aerospace and Development (AOARD 09-4045). We thank A. Becker for technical assistance. Enquiries about the PCDTBT polymer should be addressed to K.S.L., while enquiries about the photophysics should be addressed to F.L. and/or I.A.H.

■ REFERENCES

- (1) Strobel, T.; Deibel, C.; Dyakonov, V. *Phys. Rev. Lett.* **2010**, *105*, 266602.
- (2) Solarmer Energy, I. W. www.solarmer.com 2010.
- (3) Chen, H.-Y.; Hou, J.; Zhang, S.; Liang, Y.; Yang, G.; Yang, Y.; Yu, L.; Wu, Y.; Li, G. *Nat. Photon* **2009**, *3*, 649–653.
- (4) Howard, I. A.; Laquai, F. *Macromol. Chem. Phys.* **2010**, *211*, 2063–2070.
- (5) van Bavel, S. S.; Barenklau, M.; de With, G.; Hoppe, H.; Loos, J. *Adv. Funct. Mater.* **2010**, *20*, 1458–1463.
- (6) Chen, D.; Nakahara, A.; Wei, D.; Nordlund, D.; Russel, T. P. *Nano Lett.* **2010**, *11*, 7.
- (7) Muller, C.; Ferenczi, T. A. M.; Campoy-Quiles, M.; Frost, J. M.; Bradley, D. D. C.; Smith, P.; Stingelin-Stutzmann, N.; Nelson, J. *Adv. Mater.* **2008**, *20*, 3510.
- (8) Laquai, F.; Park, Y. S.; Kim, J. J.; Basche, T. *Macromol. Rapid Commun.* **2009**, *30*, 1203–1231.
- (9) Pope, M.; Swenberg, C. E. *Electronic Processes in Organic Crystals and Polymers*; Oxford University Press: Oxford, 1999.
- (10) Hertel, D.; Bässler, H. In *Organic Light Emitting Devices*; Müllen, K., Scherf, U., Eds.; Wiley-VCH: Weinheim, 2006.
- (11) Howard, I. A.; Mauer, R.; Meister, M.; Laquai, F. *J. Am. Chem. Soc.* **2010**, *132*, 14866–14876.
- (12) Guo, J.; Ohkita, H.; Benten, H.; Ito, S. *J. Am. Chem. Soc.* **2010**, *132*, 6154–6164.
- (13) Deibel, C.; Strobel, T.; Dyakonov, V. *Adv. Mater.* **2010**, *22*, 4097–4111.
- (14) Tvingstedt, K.; Vandewal, K.; Zhang, F.; Inganäs, O. *J. Phys. Chem. C* **2010**, *114*, 21824–21832.
- (15) Veldman, D.; Meskers, S. C. J.; Janssen, R. A. J. *Adv. Funct. Mater.* **2009**, *19*, 1939–1948.
- (16) Clarke, T. M.; Durrant, J. R. *Chem. Rev.* **2010**, *110*, 6736–6767.
- (17) Braun, C. L. *J. Chem. Phys.* **1984**, *80*, 4157–4161.
- (18) Onsager, L. *Phys. Rev.* **1938**, *54*, 554–557.
- (19) Wojcik, M.; Tachiya, M. *J. Chem. Phys.* **2009**, *130*, 104107.
- (20) Wojcik, M.; Michalak, P.; Tachiya, M. *Appl. Phys. Lett.* **2010**, *96*, 162102.
- (21) Shuttle, C. G.; Hamilton, R.; O'Regan, B. C.; Nelson, J.; Durrant, J. R. *Proc. Natl. Acad. Sci. U.S.A.* **2010**, *107*, 16448–16452.
- (22) Mauer, R.; Howard, I. A.; Laquai, F. *J. Phys. Chem. Lett.* **2010**, *1*, 3500–3505.
- (23) Lee, J.; Vandewal, K.; Yost, S. R.; Bahlke, M. E.; Goris, L.; Baldo, M. A.; Manca, J. V.; Voorhis, T. V. *J. Am. Chem. Soc.* **2010**, *132*, 11878–11880.
- (24) Park, S. H.; Roy, A.; Beaupre, S.; Cho, S.; Coates, N.; Moon, J. S.; Moses, D.; Leclerc, M.; Lee, K.; Heeger, A. J. *Nat. Photon* **2009**, *3*, 297.
- (25) Sun, Y.; Seo, J. H.; Takacs, C. J.; Seifert, J.; Heeger, A. J. *Adv. Mater.* **2011**, *23*, 1679–1683.
- (26) Blouin, N.; Michaud, A.; Leclerc, M. *Adv. Mater.* **2007**, *19*, 2295.
- (27) Chu, T. Y.; Alem, S.; Verly, P. G.; Wakim, S.; Lu, J. P.; Tao, Y.; Beaupre, S.; Leclerc, M.; Belanger, F.; Desilets, D.; Rodman, S.; Waller, D.; Gaudiana, R. *Appl. Phys. Lett.* **2009**, *95*, 063304.
- (28) Wakim, S.; Beaupre, S.; Blouin, N.; Aich, B. R.; Rodman, S.; Gaudiana, R.; Tao, Y.; Leclerc, M. *J. Mater. Chem.* **2009**, *19*, 5351–5358.
- (29) Street, R. A.; Cowan, S.; Heeger, A. J. *Phys. Rev. B* **2010**, *82*, 121301.
- (30) Tong, M.; Coates, N. E.; Moses, D.; Heeger, A. J.; Beaupre, S.; Leclerc, M. *Phys. Rev. B: Condens. Mater. Phys.* **2010**, *81*, 125210.
- (31) Banerji, N.; Cowan, S.; Leclerc, M.; Vauthey, E.; Heeger, A. J. *J. Am. Chem. Soc.* **2010**, *132*, 17459–17470.
- (32) Baek, N. S.; Hau, S. K.; Yip, H.-L.; Acton, O.; Chen, K.-S.; Jen, A. K. Y. *Chem. Mater.* **2008**, *20*, 5734–5736.
- (33) Burkhard, G. F.; Hoke, E. T.; Scully, S. R.; McGehee, M. D. *Nano Lett.* **2009**, *9*, 4037–4041.
- (34) Groves, C.; Blakesley, J. C.; Greenham, N. C. *Nano Lett.* **2010**, *10*, 1063–1069.
- (35) Benson-Smith, J. J.; Ohkita, H.; Cook, S.; Durrant, J. R.; Bradley, D. D. C.; Nelson, J. *J. Chem. Soc., Dalton Trans.* **2009**, 10000–10005.
- (36) Ohkita, H.; Cook, S.; Ford, T. A.; Greenham, N. C.; Durrant, J. R. *J. Photochem. Photobiol., A* **2006**, *182*, 225–230.
- (37) Clarke, T. M.; Jamieson, F. C.; Durrant, J. R. *J. Phys. Chem. C* **2009**, *113*, 20934–20941.
- (38) Guo, J.; Ohkita, H.; Benten, H.; Ito, S. *J. Am. Chem. Soc.* **2009**, *131*, 16869–16880.
- (39) Hodgkiss, J. M.; Campbell, A. R.; Marsh, R. A.; Rao, A.; Albert-Seifried, S.; Friend, R. H. *Phys. Rev. Lett.* **2010**, *104*, 177701.
- (40) Jamieson, F. C.; Agostinelli, T.; Azimi, H.; Nelson, J.; Durrant, J. R. *J. Phys. Chem. Lett.* **2010**, *1*, 3306–3310.
- (41) Blom, P. W. M.; Mihailetschi, V. D.; Koster, L. J. A.; Markov, D. E. *Adv. Mater.* **2007**, *19*, 1551–1566.
- (42) Street, R. A.; Schoendorf, M.; Roy, A.; Lee, J. H. *Phys. Rev. B* **2010**, *81*, 205307.
- (43) Cowan, S. R.; Street, R. A.; Cho, S. N.; Heeger, A. J. *Phys. Rev. B* **2011**, *83*, 035205.
- (44) Hertel, D.; Bässler, H. *ChemPhysChem* **2008**, *9*, 666–688.
- (45) Arkhipov, V. I.; Fishchuk, I. I.; Kadashchuk, A.; Bässler, H. In *Photophysics of Molecular Materials*; Lanzani, G., Ed.; Wiley-VCH: Weinheim, 2006; pp 261–366.
- (46) Laquai, F.; Wegner, G.; Bässler, H. *Philos. Trans. R. Soc. London, Ser. A* **2007**, *365*, 1473–1487.
- (47) Laquai, F.; Wegner, G.; Im, C.; Bässler, H.; Heun, S. *J. Appl. Phys.* **2006**, *99*.
- (48) Mauer, R.; Kastler, M.; Laquai, F. *Adv. Funct. Mater.* **2010**, *20*, 2085–2092.
- (49) Mihailetschi, V. D.; Koster, L. J. A.; Hummelen, J. C.; Blom, P. W. M. *Phys. Rev. Lett.* **2004**, *93*, 216601.
- (50) Moet, D. J. D.; Lenes, M.; Morana, M.; Azimi, H.; Brabec, C. J.; Blom, P. W. M. *Appl. Phys. Lett.* **2010**, *96*, 213506.
- (51) Moet, D. J. D.; Lenes, M.; Kotlarski, J. D.; Veenstra, S. C.; Sweelssen, J.; Koetse, M. M.; de Boer, B.; Blom, P. W. M. *Org. Electron.* **2009**, *10*, 1275–1281.
- (52) Deibel, C.; Strobel, T.; Dyakonov, V. *Phys. Rev. Lett.* **2009**, *103*, 036402.
- (53) Limpinsel, M.; Wagenpfahl, A.; Mingeback, M.; Deibel, C.; Dyakonov, V. *Phys. Rev. B* **2010**, *81*, 085203.